



Review

A Review on the Transport-Chemo-Mechanical Behavior in Concrete under External Sulfate Attack

Guang-Ji Yin ¹, Xiao-Dong Wen ^{1,*}, Ling Miao ², Dong Cui ³, Xiao-Bao Zuo ³ and Yu-Juan Tang ⁴

¹ School of Civil and Transportation Engineering, Ningbo University of Technology, Ningbo 315211, China

² College of Art and Design, Nanjing Forestry University, Nanjing 210037, China

³ School of Science, Nanjing University of Science and Technology, Nanjing 210094, China

⁴ School of Civil Engineering, Yangzhou Ploytechnic College, Yangzhou 225009, China

* Correspondence: nbutlsjc@126.com

Abstract: Cementitious concrete structures serving in sulfate environments suffer from serious durability challenges caused by chemical sulfate attacks (CSA), which lead to the volume expansion, cracking, and spalling of concrete and the early failure of structures. CSA on concrete involves the behaviors of ion transport, chemical reactions, the crystallization of reaction products, microstructural damage to the cement matrix, and the macroscopic deterioration of concrete, namely the transport-chemo-mechanical behaviors. This paper first introduces the reaction products, such as gypsum, ettringite, brucite, and thaumasite, between sulfate and concrete under different environmental conditions and their formation mechanism. Then, aiming at the ettringite type CSA, the theories of volume increase and crystallization pressure are elaborated to explain it-induced concrete degradation. Additionally, the crystallization pressure theory is used to describe the cracking behavior in the microstructure slurry caused by the ettringite crystal filling pore. Finally, a series of transport-chemo-mechanical models for ettringite type CSA are displaced module by module. It includes the sulfate diffusion-reaction model, the free expansion of concrete, and equivalent expansive force in concrete related to the reaction behavior: the model for chemo-mechanical behavior in concrete caused by CSA. These models can be used to analyze the distribution of sulfate ions and the reaction product content, expansive stress and strain in the concrete, and the cracking and spalling degree of the concrete, which is beneficial to evaluate the durability of concrete structures serving permanently in a sulfate environment.

Keywords: chemical sulfate attack; concrete; degradation mechanism; modeling; damage



Citation: Yin, G.-J.; Wen, X.-D.; Miao, L.; Cui, D.; Zuo, X.-B.; Tang, Y.-J. A Review on the Transport-Chemo-Mechanical Behavior in Concrete under External Sulfate Attack.

Coatings **2023**, *13*, 174. <https://doi.org/10.3390/coatings13010174>

Academic Editor: Alin Dinita

Received: 21 December 2022

Revised: 10 January 2023

Accepted: 11 January 2023

Published: 12 January 2023



Copyright: © 2023 by the authors. Licensee MDPI, Basel, Switzerland. This article is an open access article distributed under the terms and conditions of the Creative Commons Attribution (CC BY) license (<https://creativecommons.org/licenses/by/4.0/>).

1. Introduction

External sulfate attack (ESA) is an important environmental factor for durability degradation and service-life reduction in concrete structures [1,2]. According to the survey from the “China National Geographic Website” [3], the sulfate service environment in China is widely distributed. In offshore China, the sulfate content is about 1400~2700 mg/L, which causes underground soil or groundwater in coastal cities, such as Liaoning, Shandong, Jiangsu, and Zhejiang provinces, to contain a large number of sulfate ions. As a result, the service life of concrete structures such as seaports and wharves in these areas is only 25 years [4], and some of them have been severely damaged for between 7 and 20 years [5]. In Xinjiang, Qinghai, Ningxia, Gansu, Inner Mongolia, and other western regions, the sulfate content in some saline soils has reached more than 4200 mg/L, especially in the Korla area of Xinjiang, where the sulfate concentration in the groundwater is as high as 21,299 mg/L. In the Chaerhan area of Qinhai, the service life of concrete structures, such as roads, bridges, and underground pipelines, without anti-corrosion measures is only 3–5 years or even 1 year [6].

In reality, ESA is a global problem in civil engineering. As early as 1915, Wig and Williams (American Bureau of Standards) published an academic paper to report that [7]

several concrete structures exposed to saline-alkali soil or water environments in the western barren environment of the USA were to be destructed after 7 years of operation. Up to now, the research on ESA has a history of more than 120 years [8], but Adam Neville [9] pointed out in 2004 that this research was still in a confused state. He summarized two definitions of sulfate attack on concrete: one is that, as long as the interaction between the sulfate and concrete is involved, this behavior can be defined as a sulfate attack. Another is that when the chemical reaction between the sulfate ions and cement hydration products occurs and causes the expansion damage of cement paste or the durability degradation of concrete components, this behavior can be defined as a sulfate attack [10]. Obviously, the first view has a shortcoming if the sulfate in concrete does not cause any damage to the cement paste, the definition of “sulfate attack” is contrary to the essence of an “attack”. Bensted [11] considered that the generation of sulfate products and the it-induced damage of concrete are two different concepts, which should be treated differently, and therefore, Neville [9] proposed that the behaviors, without causing the degradation of concrete durability, cannot be called a sulfate attack. The second view is more reasonable in that the definition proposes two key conditions, namely, ESA inducement (sulfate reaction products) and ESA consequence (expansion and degradation of concrete). As Harrison and Cooke [12] pointed out, although there is a large amount of sulfate ion entering into concrete or reaction products generated in the concrete, it does not mean the occurrence of ESA. Only strength decline or other damage characteristics in the concrete can be further observed, which can provide effective evidence for ESA.

However, it can be known from the above definition that the ESA refers in particular to the chemical sulfate attack (CSA), and correspondingly, another kind of ESA is the physical sulfate attack (PSA). Under specific environmental conditions similar to the drying-wetting alternation and periodic temperature change, the repeated dissolution-crystallization action of sulfate, which causes the fatigue failure of concrete [8]. This sulfate crystallization behavior does not involve the chemical reaction of substances in concrete.

In this paper, the behavior (sulfate transport-chemo-mechanical behavior) of CSA on concrete is the main discussion object. The degradation of concrete structures caused by CSA is the result of long-term corrosion, and the model prediction is a necessary analysis method for the CSA-induced durability problem. To clearly describe the current research status of the CSA model, the reaction products of CSA, their formation mechanism, and them-induced failure forms of concrete are first described simply. Most of these studies were completed between the 1980s and 1990s, and a few were developed after the 2000s. Then, the numerical model for CSA behaviors is presented module by module. It involves the diffusion of sulfate ions, chemical reactions, the it-induced volume expansion of concrete, crystallization pressure in the pore solution, and mechanical responses (expansive stress, strain, damage degree) in the concrete, and most of these works were carried out after 2000. The framework of this paper is shown in Figure 1.

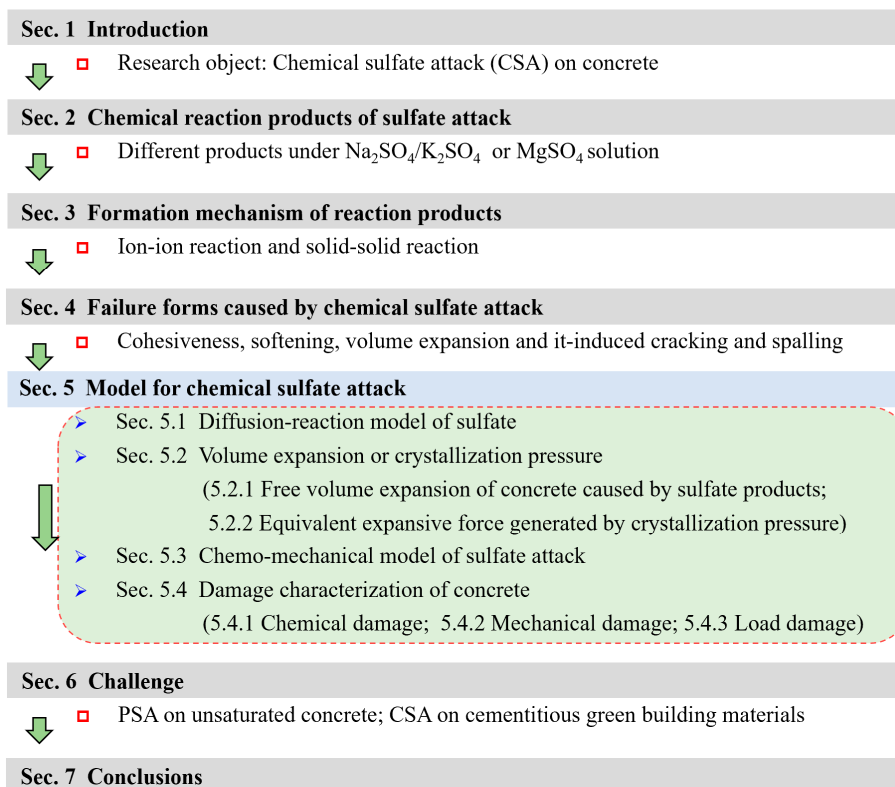


Figure 1. Framework of the review.

2. Chemical Reaction Products of Sulfate Attack

The important characterization of CSA on concrete is the microstructure damage of cement paste caused by the growth of sulfate reaction products. Modern microscopic measurements, such as scanning electron microscope (SEM), X-ray diffraction (XRD), and mercury intrusion porosimetry (MIP), are utilized to observe the microstructure evolution of cement paste. The results show that the sulfate products form in micropores, including gypsum ($\text{C}\bar{\text{S}}\text{H}_2$) [13,14], ettringite ($\text{C}_6\text{A}\bar{\text{S}}_3\text{H}_{32}$) [15–17], and thaumasite ($\text{C}_3\text{S} \cdot \text{C}\bar{\text{S}}\text{H}_{15}$) [18–20], accompanied by the propagation of microcracks.

In reality, the types of sulfate products are affected by corrosion conditions, such as the solution concentration, pH value, ambient temperature, and cation type. Biczok [21] found that if the concentration of the sodium sulfate solution is lower than 1000 mg/L, the main product is ettringite, while it is mainly gypsum if the concentration is higher than 8000 mg/L. Bellmann [22] found that the greater the pH value of the solution, the higher the sulfate concentration required for gypsum formation. The minimum sulfate concentration required for gypsum formation is about 1400 mg/L, and the corresponding pH of the solution is 12.45. When the pH value rises to 12.9, sulfate ions hardly react with calcium hydroxide to form gypsum. Some studies [19,23,24] pointed out that thaumasite will be formed preferentially in a low-temperature ($\leq 15^\circ\text{C}$) humid environment with a pH value higher than 10.5 and the appropriate amount of CO_2 or CO_3^{2-} . However, it is observed in some on-site engineering investigations with a temperature $\geq 20^\circ\text{C}$ [25,26] that, for cation type, the products of magnesium sulfate attack are different from that of other common basic ions such as Na^+/K^+ [27–29], as shown in Figure 2 [30]. Besides gypsum and ettringite, the insoluble brucite, $\text{Mg}(\text{OH})_2$, is also formed to cause a decrease in the pH value of pore solutions and the decalcification of C-S-H gel, which becomes the cohesionless silica gel, $\text{SiO}_2 \cdot x\text{H}_2\text{O}$, or magnesium silicate, $3\text{MgO} \cdot 2\text{SiO}_2 \cdot 2\text{H}_2\text{O}$. In short, sulfate products are different in different corrosion environments.

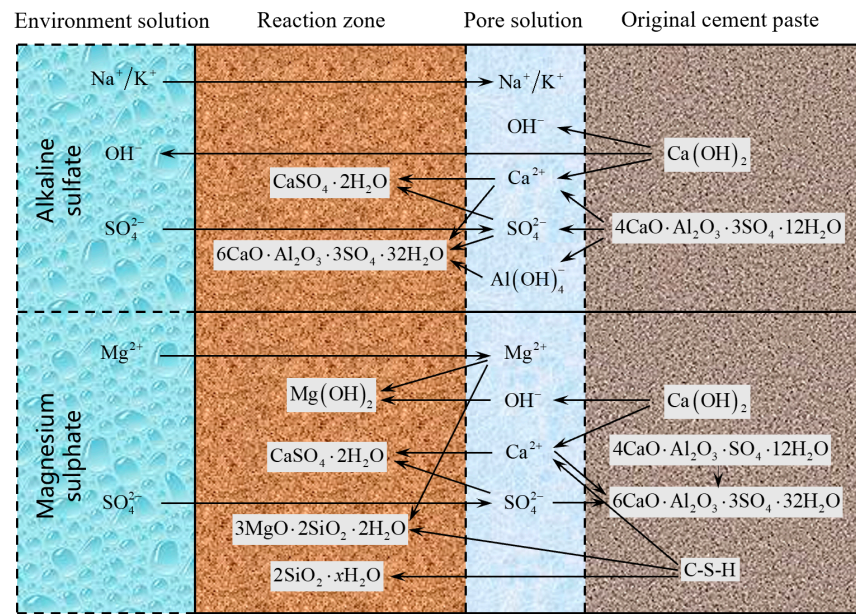


Figure 2. Chemical reactions in concrete under different cation sulfates [30].

3. Formation Mechanism of Reaction Products

The formation mechanism of sulfate reaction products, including gypsum, ettringite, thaumasite, and brucite is different, even controversial. In different references, the description of their reaction mechanism is inconsistent, similar to ion–ion reactions for gypsum, through-solution [31,32] or the topochemical [33,34] mechanism for ettringite, the direct [35] or indirect [36] reaction for thaumasite, and ion–ion reactions for brucite, presented in Table 1. It can be seen from the chemical reaction equations in this table that the essence of through-solution and direct reaction is the ion–ion reactions in pore solution, and that of topochemical and indirect reaction is the solid–solid reaction in the cement matrix.

Table 1. Reaction equations and formation mechanisms of products in concrete.

| Cation Type | Sulfate Product | Formation Mechanism | Chemical Reaction |
|---------------------------------|-----------------|---|---|
| Na ⁺ /K ⁺ | Gypsum | Ion–ion reaction | $Ca^{2+} + SO_4^{2-} + 2H_2O \rightarrow C\bar{S}H_2$ |
| | Ettringite | Topochemical mechanism (Solid–solid reaction) | $\left\{ \begin{array}{l} \text{Equation (a): } C_4AH_{13} + 3C\bar{S}H_2 + 14H_2O \rightarrow C_6A\bar{S}_3H_{32} + CH \\ \text{Equation (b): } C_4ASH_{12} + 2CSH_2 + 16H_2O \rightarrow C_6A\bar{S}_3H_{32} \\ \text{Equation (c): } C_3A + 3C\bar{S}H_2 + 26H_2O \rightarrow C_6A\bar{S}_3H_{32} \end{array} \right.$ |
| | | Through-solution mechanism (Ion–ion reaction) | $\left\{ \begin{array}{l} Al(OH)_4^- + 2OH^- \rightarrow [Al(OH)_6]^{3-} \\ [Al(OH)_6]^{3-} + 3Ca^{2+} + 12H_2O \rightarrow [Ca_3Al(OH)_6 \cdot 12H_2O]^{3+} \\ 2[Ca_3Al(OH)_6 \cdot 12H_2O]^{3+} + 3SO_4^{2-} + 2H_2O \rightarrow C_6A\bar{S}_3H_{32} \end{array} \right.$ |
| | Thaumasite | Direct reaction (Ion–ion reaction) | $SO_4^{2-} + 3Ca^{2+} + CO_3^{2-} + SiO_3^{2-} + 15H_2O \rightarrow C_3S \cdot C\bar{S}H_{15}$ |
| | | Indirect reaction (Solid–solid reaction) | $C_3S_2H_3 + C_6A\bar{S}_3H_{32} + 2C\bar{C} + 4H \rightarrow 2(C_3S \cdot C\bar{S}H_{15}) + C\bar{S}H_2 + AH_3 + 4CH$ |
| Mg ²⁺ | Brucite | Ion–ion reaction | $\left\{ \begin{array}{l} Mg^{2+} + SO_4^{2-} + Ca^{2+} + 2OH^- + 2H_2O \rightarrow MH + C\bar{S}H_2 \\ aMg^{2+} + aSO_4^{2-} + aCaO \cdot SiO_2 \cdot xH_2O + 2H_2O \rightarrow aMH + aC\bar{S}H_2 + SH_x \\ 2aMg^{2+} + 2aSO_4^{2-} + 2(aCaO \cdot SiO_2 \cdot xH_2O) + (6a - 1 - 2x)H_2O \rightarrow (2a - 3)MH + 2aC\bar{S}H_2 + M_3S_2H_2 \end{array} \right.$ |

$H_2O \rightarrow H$; $Ca(OH)_2 \rightarrow CaO \cdot H_2O \rightarrow CH$; $2Al(OH)_3 \rightarrow Al_2O_3 \cdot 3H_2O \rightarrow AH_3$; $CaSO_4 \cdot 2H_2O \rightarrow CaO \cdot SO_3 \cdot 2H_2O \rightarrow C\bar{S}H_2$; $CaCO_3 \rightarrow CaO \cdot CO_2 \rightarrow C\bar{C}$; $Mg(OH)_2 \rightarrow MgO \cdot H_2O \rightarrow MH$; $SiO_2 \cdot xH_2O \rightarrow SH_x$; $3MgO \cdot 2SiO_2 \cdot 2H_2O \rightarrow M_3S_2H_2$.

4. Failure Forms Caused by Chemical Reaction Attack

According to the difference in sulfate products, the CSA can be classically divided into gypsum type, ettringite type, thaumasite type CSA in the case of Na^+/K^+ , and brucite type CSA in the case of Mg^{2+} . The different types of CSA present different failure forms of concrete, including softening, cohesiveness, volume expansion, and its-induced cracking/spalling [37,38]. Table 2 shows the relationship between cation types of sulfate solution, CSA classification, and failure forms of concrete. It should be pointed out that the third failure form is the most common among them. At the initial stage of CSA, there are two major disputes about the degradation of concrete exposed to the sulfate environment, namely “degradation cause” and “degradation mechanism”. The former refers to which reaction product (gypsum or ettringite) is the main cause of concrete expansion/cracking, while the latter indicates how CSA causes concrete degradation.

Table 2. Relationship among cation type of sulfate solution, CSA classification, and failure forms.

| Cation Type | | CSA Type/Sulfate Product | | | |
|--------------------------|--|---|----------|------------|----------|
| | | Thaumasite | Gypsum | Ettringite | Brucite |
| Na^+/K^+ | | √ (CO_2 or CO_3^{2-}) | √ (main) | √ (main) | |
| Mg^{2+} | | | √ | √ | √ (main) |
| Failure form | Cohesiveness | ○ | | | ○ |
| | Softening | | ○ | | |
| | Volume expansion and its-induced cracking/spalling | | ○ | ○ | |

4.1. Degradation Cause of Concrete

In the early period of research on CSA, many scholars, such as Mehta, Tian and Cohen, Mather, Hansen, Collepard [39], Brown and Taylor et al. [31], believed that the volume expansion of concrete exposed to a sulfate environment was caused by the ettringite growth. Subsequently, some scholars, including Metha, Cohen [14], and Santhanam et al. [13], carried out the corrosion experiment of cement paste/mortar specimens immersed in the sulfate solution to investigate the effect of gypsum formation on the failure of cement-based materials. In these studies [13,14], C_3S cement with low C_3A content was used to reduce the source of the aluminum phase required for ettringite formation, thereby minimizing the amount of ettringite formation. The results showed that the C_3S cement specimen soaked in sulfate solution for a long time occurred macroscopic damage phenomena, such as volume expansion and surface cracking, mass, and strength loss. Additionally, the expansion deformation of the C_3S cement specimen is obviously greater than that of the Portland cement specimen. Therefore, the formation of ettringite and gypsum is the main cause of the volume expansion or cracking of concrete subjected to CSA.

4.2. Degradation Mechanism of Concrete

Although the solid volume increase to 1.2 times that of the original form of calcium hydroxide transforming into gypsum, the research focus at that time was still on the expansion and deterioration of concrete caused by ettringite. It was believed that the gypsum formation mainly played a role in softening concrete and filling micro-cracks. So, the degradation mechanisms of concrete under CSA, including the theories of volume increase [40], topochemical reaction [41,42], water swelling [43], and crystallization pressure [44,45], are mostly proposed for ettringite type CSA.

The theory of volume increase considers that when the calcium aluminate (CA) in concrete is converted into ettringite, the volume of the solid phase increases 2.5 times, causing the significant expansion of the concrete. This theory seems to be the simplest degradation mechanism, so it is adopted by most scholars to model the behavior of CSA [46]. However, through thermodynamic calculation, Lothornbach [47] and Kunther [48] found

that the total volume of products (ettringite) did not exceed the total volume of reactants (for the case of 2.5 times, water was consumed as the reactant). Additionally, there is no experimental evidence to prove the direct relationship between ettringite production and the volume expansion of concrete [37,49]. The theory of topochemical reaction refers to that; ettringite is directly converted from the surface of CA crystal through solid–solid reactions. However, the crystal structure of both hydrated and unhydrated C_3A is irrelevant to that of ettringite, which means that it is difficult to achieve the above transformation at room temperature [37,50]. In reality, SEM observation shows that ettringite is not found at the location of C_3A hydrated products and on the surface of unhydrated C_3A particles. Water swelling refers to the fact that, in the condition of the saturated lime solution, the gel-like and small ettringite colloid can be formed in concrete. This kind of colloid with a large specific surface area can absorb a large number of water molecules, resulting in the volume expansion of concrete [43]. However, Scrivener [50] believes that ettringite generated in concrete subjected to a sulfate attack is a typical crystal, and it is impossible to absorb a lot of water.

At present, the theory of crystallization pressure developed in recent years can reasonably explain the CSA-induced expansion and damage of concrete. As early as 1949, based on thermodynamic theory, Correns deduced the calculation formula of salt crystallization pressure [51], expressed as Equation (1). Subsequently, Scherer [42,43], Steiger [52,53], Espinosa [54], and Komiorczyk [55] et al. developed the theory of crystallization pressure and pointed out that the “supersaturated concentration of solution” and “relatively closed small space” are two key factors for the generation of crystallization pressure. Flatt et al. [56] found that when ettringite was formed in a pore with a size smaller than about 100 nm, the generated crystallization pressure due to the supersaturated solution caused the cracking of cement paste. Müllauer et al. [57] found that, under the immersion of the 30 g/L sodium sulfate solution, the maximum crystallization pressure in cement mortar reached 7–8 MPa, while the pore diameter in the mortar was about 23–27 nm.

$$P_c = \frac{RT}{v_{\text{mol}}} \ln \beta \quad (1)$$

where P_c is the crystallization pressure; R is the ideal gas constant; T is the absolute temperature; v_{mol} is the molar volume of ettringite crystal; β is the solution supersaturation.

Furthermore, Scherer [44,45], Steiger [52,53], and Müllauer [57] also pointed out that the crystallization pressure in a single pore, exceeding the materials’ tensile strength, cannot cause the destruction of porous materials such as cement mortar and concrete. However, the equivalent expansion stress in the local area of porous materials caused by crystallization pressure in multiple pores will result in the macroscopic expansion and cracking of a porous material. In the process of CSA, there are several connected pores with different space sizes in the local area of concrete, while their solution supersaturations are the same. According to the crystallization pressure theory, the crystals in these pores with the same supersaturation pore solution have the same curvatures/sizes in the equilibrium state, and a smaller crystal (with a large curvature) needs higher supersaturation to maintain its size [57]. If there are two crystals with different sizes in the same pore solution, the small crystal dissolves first, and the solute molecules transfer to the large crystal, resulting in an increase in its size [58]. Thus, with the increase in pore solution saturation, ettringite first crystallizes in big pores. After the big pore is filled to a certain extent, the crystals continue to fill into small pores; that is, small pores are filled after big ones [57], as shown in Figure 3. Meanwhile, the crystallization pressure increases to cause macroscopic damage to concrete.

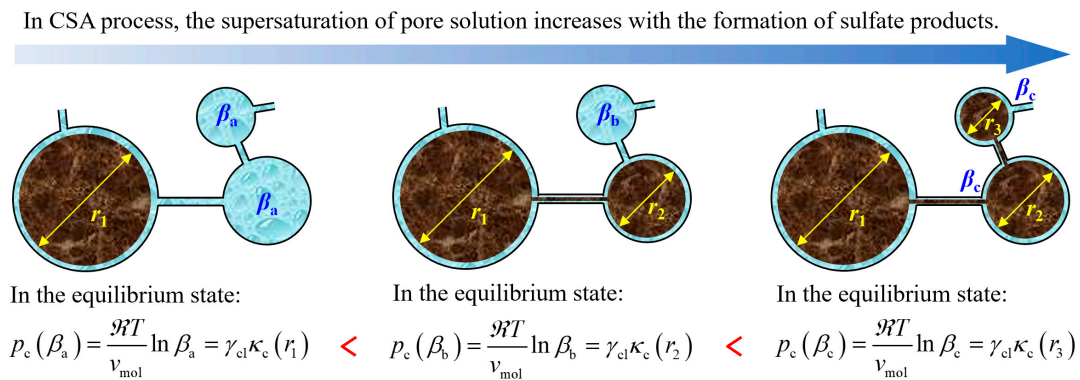


Figure 3. Filling behavior of ettringite crystal in pore system of local concrete.

(In equilibrium state: the higher the solution supersaturation required to maintain smaller crystals, the crystallization pressure driven by supersaturated solution is greater.)

5. Model for Chemical Sulfate Attack

5.1. Diffusion-Reaction Model of Sulfate

Due to the complexity of CSA and the limitations of its mechanism at the early stage of this research, it is difficult to directly establish a diffusion-chemo-mechanical model for numerically simulating the whole failure process of CSA on concrete. So, the scholars first obtained the distribution of sulfate ion concentration in concrete through EDTA titration and EDS quantitative analysis. Then, based on the experimental data, the diffusion-reaction model of sulfate ions in concrete was built up to analyze the behavior of CSA by using Fick's law, chemical reaction kinetics, and thermodynamics. The basic equation is expressed as Equation (2), which is summarized from the works by Yin et al. [59], Guan et al. [60], Zhao et al. [61], Ran et al. [62], Zou et al. [63], Yu et al. [64], and Wang et al. [65].

$$\frac{\partial C}{\partial t} = -\nabla J + k_r C, \quad J = D \nabla C \quad (2)$$

in which C is the sulfate ion concentration in concrete, J is the sulfate ion flow in concrete, D is the effective diffusion coefficient of the sulfate ion in concrete, $k_r C$ respects the reaction consumption of sulfate ion, and ∇ is the Hamilton operator. It should be pointed out that the diffusion coefficient D is a spatiotemporal variable, so Equation (2) is a non-steady equation and can be solved by a numerical solution [59], such as the finite difference method, finite volume method, or finite element method, etc. In the works of Guan et al. [60] and Zhao et al. [61], D is regarded to be a constant, so Equation (2) can be expressed as

$$\frac{\partial C}{\partial t} = -D \Delta C + k_r C \quad (3)$$

where Δ is the Laplace operator, and Equation (3) can be solved analytically by using Laplace transform.

Equation (2) or (3) is only applied to the diffusion behavior of the sulfate ion in saturation concrete, driven by the concentration gradient, and the term of $J = D \nabla C$ represents the diffusion behavior. Furthermore, the sulfate ion transport is affected by other factors [63–65], such as liquid advection, ion–ion interactions, the electrical field, temperature effect, etc. So, the term of $J = D \nabla C$ in Equation (2) is usually corrected as in Table 3.

Table 3. Influence factors of sulfate ion transport in concrete.

| Basic Form | | $\frac{\partial C}{\partial t} = \underbrace{-\nabla J}_{\text{Ion transport}} + \underbrace{k_r C}_{\text{Chemical consumption}}$ |
|-----------------------|--|--|
| Ion flow | Diffusion behavior | $J = D \nabla C$ |
| | Mutual restriction effect between charged ions | $J = DC \nabla \Psi$ |
| | Influence of ionic chemical activity | $J = DC \nabla (\ln \gamma)$ |
| | Ion migration effect with solution convection | $J = Cv$ |
| | Temperature effect | $J = \frac{DC}{T} \nabla T$ |
| | Coupled by the above factors | $J = D \nabla C + DC \nabla \Psi + DC \nabla (\ln \gamma) + Cv$ |
| Effective diffusivity | Temperature effect | $D = \begin{cases} D_{c-\min} + \left(\underbrace{D_{c0}(T)}_{\text{Temperature}} - \underbrace{D_{c-\min}}_{\text{Product filling}} \right) \underbrace{f(\varphi)}_{\text{Porosity}} \\ \text{or } \underbrace{D_{cr}(\sigma)}_{\text{Crack effect (stress)}} \\ \text{or } D_w \cdot \underbrace{\varphi(\sigma)}_{\text{Load}} \cdot \underbrace{\tau(\sigma, \varphi)^{-1}}_{\text{Load, tortuosity}} \\ \text{or } D_{c0} \left(\underbrace{\varphi(w)}_{\text{hydration}} + \underbrace{d(C, t)}_{\text{ESA-induced damage}} \right) \end{cases}$ |
| | Sulfate products filling in pore | |
| | ESA-induced microcrack effect | |
| | Damage degree | |
| | Cement hydration | |

J is the ion flow in concrete; D is the effective diffusivity of sulfate ion in concrete; C is the sulfate ion concentration in concrete; the term $k_r C$ is the consumption of sulfate ion due to chemical reaction in concrete; the term $\nabla \Psi$ reflects the effect of Electric field; the term $\nabla (\ln \gamma)$ reflects the influence of ionic chemical activity; v is the solution flow rate; d is the damage degree; φ is the porosity; τ is the tortuosity; T is the temperature; σ is the stress.

Gospodinov [66,67] built up a two-dimensional non-steady diffusion model of sulfate ions by considering the effect of reaction consumption between sulfate ions and cement hydration products on the transport process. Later, he [68] further considered the influence of the sulfate products' precipitation and liquid pressure in pores on the ion effective diffusivity and established a three-dimensional non-steady diffusion model. Marchand [69] considered the coupling effect of ion transport and solution advection in saturated concrete and the chemical equilibrium of solid phase decomposition and established a STADIUM mathematical model. This model can be used to analyze the effects of the water-cement ratio, cement type, solution concentration, and environmental humidity on sulfate ion transport behavior.

Besides the ion transport form, the effective diffusivity D is also a major parameter of the transport process of ions in concrete. It is mainly related to the microstructure characteristics of concrete (such as porosity φ and tortuosity τ) and the ion diffusivity in water, while they are also affected by various factors, including the temperature, the sulfate products filling in the pore [70] (as shown in Figure 4), the damage degree, and the ESA-induced microcrack effect, etc., as listed in Table 3. Zuo et al. [71,72] considered the influence of external load on the tortuosity and porosity of concrete, established two- and three-dimensional non-steady diffusion-reaction models of sulfate ions, and used the ADI scheme of the finite difference method for its numerical solution. Sun et al. [73] carried out experiments to investigate the influence of the CSA-induced damage degree on the transport process of sulfate ions in concrete and integrated it into a new ion diffusion model. The above model can numerically calculate the time-varying concentration of sulfate ion in concrete but cannot analyze the CSA-induced mechanical response and damage degree of the concrete.

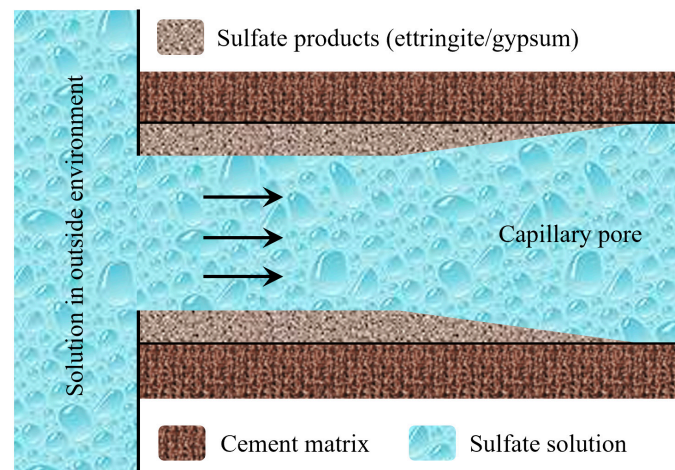


Figure 4. Filling of sulfate products in pore [70].

In the above transport model, the concept of the effective diffusion coefficient is introduced from the perspective of macro homogeneity materials to facilitate modeling. In reality, concrete is a heterogeneous random multiphase material with different ion diffusion properties in each phase, such as cement paste, aggregate, and the interface transition zone (ITZ). In recent years, there has been considerable research into the influence of ITZ on ion diffusivity in concrete. Yang et al. [74] found that the thickness of ITZ and the water cement ratio has an obvious effect on the ion diffusivity. When the thicknesses of ITZ is 20, 40, and 50 μm , the diffusion coefficients of chloride ion in it are 2.83, 1.75, and 1.55 times them in the cement matrix. In the cases of water-cement ratio 0.35, 0.45, and 0.55, the diffusion coefficients in ITZ were 27.1, 29.8, and 34 times them in the cement matrix [75]. Additionally, Huang et al. [76] found that the water transfer performance in ITZ is also related to the type and material of aggregate, and its ratio between ITZ and cement matrix is about 90–175, and it decreases with the increase in the sand cement ratio. By considering the difference in the transport property of ITZ and the cement matrix, the progress of water transport, ion diffusion, or chemical sulfate attack in concrete can be better predicted.

5.2. Volume Expansion or Crystallization Pressure

5.2.1. Free Volume Expansion of Concrete Caused by Sulfate Products

The volume expansion of concrete is always aimed at ettringite type CSA. As described above, the viewpoint of the ettringite formation mechanism has two kinds, namely the solid–solid reaction and ion–ion reaction, while most of the computational analysis is based on the former. In early research, Atkinson and Hearned [77] put forward an empirical model to describe the relationship between the expansion deformation of the concrete and the amount of ettringite formation by summarizing the experimental data. Clifton and Pommershein [46] studied the volume change caused by various chemical reactions between sulfate ion and cement hydration products and also proposed a prediction model for the volume expansion of cement-based materials subjected to CSA, in which the expansion degree has a linear relationship with the amount of ettringite generated.

In order to facilitate the calculation of ettringite production, the chemical reactions of ettringite formation, namely Equations (a)–(c) in Table 1, are simplified into a unified formula, expressed as Equation (4) [78].



in which CA respects the hydrated calcium aluminates (C_4AH_{13} and $\text{C}_4\text{A}\bar{\text{S}}\text{H}_{12}$) in cement hydration products and unhydrated tricalcium aluminate (C_3A). q is the equivalent reaction coefficient of ettringite produced by gypsum consumption, which is equal to 8/3. In reality, the gypsum formation from the sulfate ion and calcium ion, provided by the

dissolution of solid calcium (calcium hydroxide and C-S-H gel), also causes the volume expansion of concrete.

The coefficient of the volume change for each chemical reaction to generate ettringite can be calculated by the molar volume of materials before and after the reaction, as in Equation (5). The coefficient value of the volume change in concrete is given in Table 4 [78].

$$\frac{\Delta V_i}{V_i} = \frac{\nu_{\text{mol-Ett}}}{\nu_{\text{mol-CA}_i} + \gamma_i \nu_{\text{mol-Gyp}}} - 1 \quad (5)$$

In which $i = 1, 2, 3$ correspond, in turn, to the reaction Equations (a)–(c) in Table 1. ΔV_i and V_i are the volume change caused by the chemical reaction i and the total volume of substances before reaction, respectively. $\nu_{\text{mol-Ett}}$, $\nu_{\text{mol-CA}_i}$, and $\nu_{\text{mol-Gyp}}$ represent the molar volumes of ettringite, calcium aluminate, and gypsum; γ_i ($i = 1, 2, 3$) are the reaction coefficients of reaction Equations (a)–(c), respectively.

Table 4. Coefficients of volume change in concrete caused by chemical reactions.

| Chemical Reactions | $\Delta V_i/V_i$ |
|--|------------------|
| Equation (a) : $C_4AH_{13} + 3\bar{C}SH_2 + 14H_2O \rightarrow C_6\bar{A}S_3H_{32} + CH$ | 0.48 |
| Equation (b) : $C_4ASH_{12} + 2\bar{C}SH_2 + 16H_2O \rightarrow C_6\bar{A}S_3H_{32}$ | 0.51 |
| Equation (c) : $C_3A + 3\bar{C}SH_2 + 26H_2O \rightarrow C_6\bar{A}S_3H_{32}$ | 1.26 |

Due to the existence of capillary pores in the concrete, sulfate products first fill the pore space. However, a large number of SEM observations on the microstructure of failure concrete subjected to sulfate attacks found that the sulfate products such as gypsum and ettringite do not fill the entire cracked pores. In other words, if the pores are filled to a certain extent, the continuous generation of sulfate products causes the volume expansion of the concrete. In many references, the parameters of the critical filling volume fraction of pore, f , are introduced to describe the above filling effect, and its empirical value may be 0.05–0.45 by Tixier and Mobasher [78], 0.5 by Basista and Wegnewski [79], 0.05 by Idiart [80], 0.1 by Ikumi [81], and 0.3 by Yu [64]. So, the free volume expansion of concrete caused by sulfate products [64,81], without considering the restraint effect of the hole wall, can be calculated as:

$$\varepsilon_V = \max \left\{ \frac{1}{q} \sum_{i=1}^3 \left(\frac{\Delta V_i}{V_i} \frac{1}{\nu_{\text{mol-CA}_i}} - \frac{\gamma_i}{\nu_{\text{mol-CA}_i}} \right) C_{CA} - f\varphi_0, 0 \right\} \quad (6)$$

where C_{CA} is the concentration of CA in the concrete; φ_0 is the initial porosity in the concrete.

5.2.2. Equivalent Expansive Force Generated by Crystallization Pressure

The crystallization pressure driven by pore solution supersaturation is the alternative view for concrete degradation under CSA. It should be pointed out that the volume expansion for concrete failure is a phenomenological viewpoint, while the crystallization pressure, based on the thermodynamic theory, seems to be more scientific and systematic [82]. However, the mechanical analysis of concrete under CSA uses the crystallization pressure theory. A possible reason is the lack of such a bridge between local damage around the pores and the global failure of concrete [83].

As pointed out by Scherer [45], the concrete matrix around the pore will crack once the crystallization pressure on the pore wall is beyond its tensile strength, but only the synergistic damage of the multiple pores' local area will cause the failure of the whole element or component. Therefore, it is necessary to think about the equivalent expansive force generated by crystallization pressure in the concrete element or component. In the authors' incomplete statistics, Bary [84] (published in 2008, after Sherer 1999 [44], 2004 [45]) first analyzed the mechanical behavior of concrete caused by CSA from the perspective of crystallization pressure. In this research, the expansion-induced cracking of the concrete is

attributed to the crystallization pressure generated by the ettringite growth in the pores, and the equivalent expansive force, P_{eff} , in concrete is calculated by crystallization pressure [84] as:

$$P_{\text{eff}} = \alpha_{\text{AFm}} p_c \quad (7)$$

where α_{AFm} is the interaction coefficient between the ettringite crystallization growth and concrete matrix constraint.

Feng et al. [85] analyzed the microstructure mechanical response in the cement paste by crystallization pressure and established the quantitative relation among the crystallization pressure, localized stress-free strain, and equivalent expansive stress, namely $P_{\text{eff}} \sim \varepsilon_{\text{free}} \sim p_c$. Basista and Weglewski [79] presented the calculation formula of the equivalent expansive force to describe the propagation of cracks in concrete, but the P_{eff} is obtained from the expansion strain of sulfate product growth, namely $P_{\text{eff}} \sim \varepsilon_V$ [calculated as Equation (6)].

5.3. Chemo-Mechanical Model of Sulfate Attack

On the basis of more clear degradation mechanisms of CSA and the sulfate diffusion-reaction model, scholars have established a series of chemo-mechanical models to describe the whole process of the expansion-induced degradation of concrete under CSA by using continuum damage mechanics, micropore mechanics, and thermodynamic theory, etc. Table 5 lists some achievements in the research on chemo-mechanical models in recent years.

Table 5. Chemo-mechanical models for concrete subjected to CSA.

| Author | Published Time | Degradation Cause | Degradation Mechanism |
|-----------------------------|----------------|--------------------|---|
| Tixier and Mobasher [78,86] | 2003 | Ettringite | Volume increase theory |
| Bary [84] | 2008 | Ettringite, Gypsum | Crystallization pressure theory |
| Bary et al. [87] | 2014 | Ettringite | Volume increase theory, crystallization pressure theory |
| Basista and Weglewski [79] | 2009 | Ettringite | Volume increase theory |
| Sarkar et al. [88] | 2010 | Ettringite | Volume increase theory |
| Sarkar et al. [89] | 2012 | Ettringite, Gypsum | Volume increase theory |
| Idiart et al. [80] | 2011 | Ettringite | Volume increase theory |
| Ikumi et al. [81] | 2014 | Ettringite | Volume increase theory |
| Ikumi et al. [90] | 2016 | Ettringite | Volume increase theory |
| Cefis and Comi [91] | 2014 | Ettringite | Volume increase theory |
| Cefis and Comi [92] | 2017 | Ettringite | Volume increase theory |
| Zuo et al. [93] | 2009 | Ettringite | Volume increase theory |
| Zuo et al. [94] | 2012 | Ettringite | Volume increase theory |
| Nie et al. [95] | 2015 | Ettringite | Volume increase theory |
| Yin et al. [96] | 2017 | Ettringite, Gypsum | Volume increase theory |
| Yin et al. [97] | 2019 | Ettringite | Crystallization pressure theory |
| Yu et al. [64] | 2018 | Ettringite | Volume increase theory |
| Yu et al. [98] | 2021 | Ettringite | Volume increase theory |
| Yi et al. [99] | 2019 | Ettringite | Volume increase theory |

In the above research, the model proposed by Tixier and Mobasher [78,86] is the most classic, in which the growth of ettringite in the cement paste is regarded as an inclusion problem. Using the theory of volume increase, they obtained the free expansion strain caused by the ettringite growth and analyzed the macroscopic stress and strain in the concrete in combination with the simplified uniaxial tensile stress–strain relationship. In addition, by taking the residual calcium aluminate (CA) concentration at the initial cracking

moment as the critical threshold concentration, the corresponding boundary movement criterion was proposed.

On the basis of Tixier and Mobasher [78,86], Sarkar et al. [88] established a mathematical model to simulate the deterioration process of concrete under CSA. In the model, the diffusion behavior of ions from outside to inside and the calcium leaching effect from inside to outside were synchronously considered as reflecting this coupled influence on the chemical reaction balance. The basic mechanical equation or constitutive equation of the model is written as Equation (9).

Bary et al. [84] attributed the concrete damage to the crystallization pressure generated by the growth of ettringite and gypsum and the volume expansion of cement paste around the micropores. By simultaneously introducing a free volume expansion strain and crystallization pressure, they established a more reasonable transport-chemo-mechanical model, and the basic mechanical equation is expressed as Equation (10).

Cefis and Comi [92] studied the mechanical response of partially or fully saturated concrete structures under sulfate attack and proposed a weak coupling analysis method. First, the water content in the cement paste was obtained through a simplified diffusion model; secondly, using the diffusion-reaction model, the concentrations of the sulfate ions and sulfate products were calculated. Finally, considering the water pressure on the pore wall, a multiphase elastic-damage model coupled with chemo-mechanical damage was established to analyze the nonlinear mechanical response of concrete under CSA, presented in Equation (11).

Other chemo-mechanical models are much the same, and the basic framework is also improved on the basis of the Tixier and Mobasher model [78,86]. The specific mechanical equations are shown in Table 6.

Table 6. Basic constitutive equations in the chemo-mechanical models.

| Authors | Basic Mechanical Equation | Number |
|-------------------------|---|--------|
| Saetta et al. [100,101] | $\sigma = \underbrace{(1 - d_c)}_{\text{Chemical damage}} \cdot \underbrace{(1 - d_l)}_{\text{Load damage}} \cdot C_0 : \varepsilon$ <p>d_c is the CSA-induced chemical damage. d_l is the loading damage caused by external loading. This model can be used to analyze the stress in concrete under the external load and environment corrosion.</p> | (8) |
| Sarkar et al. [88] | $\sigma = \underbrace{(1 - d_c)}_{\text{Chemical damage}} \cdot E_0 \cdot \underbrace{\varepsilon}_{\text{Related to free expansion } \varepsilon_V}, \quad d_c = f(\varepsilon)$ <p>In sarkar’s model, the ε is calculated by the free expansion and ε_V is caused by the growth of sulfate products.</p> | (9) |
| Bary et al. [87] | $\sigma = \underbrace{(1 - d_c)}_{\text{Chemical damage}} \cdot \left[C_0 : \left(\varepsilon - \underbrace{\varepsilon_{es}}_{\text{Related to free expansion } \varepsilon_V} \right) - \underbrace{\alpha_{AFm} p_c \mathbf{1}}_{\text{Crystallization pressure}} \right]$ <p>The effects of crystallization pressure and free expansion are considered together in the model.</p> | (10) |
| Cefis and Comi [92] | $\sigma = \underbrace{(1 - d_c)}_{\text{Chemical damage}} \cdot \underbrace{(1 - d_m)}_{\text{Mechanical damage}} \cdot [2G\varepsilon + Ktr\varepsilon \mathbf{1}] - \underbrace{bp_w \mathbf{1}}_{\text{Hydrostatic pressure}}$ <p>In this model, the CSA-induced mechanical and chemical damages are considered. Additionally, the hydrostatic pressure p_w is introduced in the basic constitutive equation. So, this model is applicable to the case of sulfate attack on unsaturated concrete.</p> | (11) |
| Ikumi et al. [81] | $\sigma = \underbrace{(1 - d_c)}_{\text{Chemical damage}} \cdot E_0 \cdot \left(\varepsilon - \underbrace{\varepsilon_{non-mech}}_{\text{Related to free expansion } \varepsilon_V} \right)$ <p>Ikumi’s model is similar to that of Sarkar, but he considered the influence of pore size on ε_V.</p> | (12) |

Table 6. Cont.

| Authors | Basic Mechanical Equation | Number |
|--|---|--------|
| Yin et al. [96] | $\sigma = \underbrace{(1 - d_l)}_{\text{Load damage}} \underbrace{(1 - d_c)}_{\text{Chemical damage}} C_0 : (\varepsilon - \varepsilon_p)$ | (13) |
| Yin et al. [102] | $\sigma = \underbrace{(1 - d_c)}_{\text{Chemical damage}} C_0 : \left(\varepsilon - \varepsilon_p - \underbrace{\varepsilon_{EG}}_{\text{Related to free expansion } \varepsilon_V} \right)$ | (14) |
| In Yin’s models, the chemical damage d_c is analyzed by using the elastoplastic damage mechanics, not determined by the empirical formula related to the content of sulfate ion or the reaction product. | | |

5.4. Damage Characterization of Concrete

In the chemo-mechanical models, the damage variables are introduced in the basic mechanical equations (in Table 6) to describe the actual mechanical response in the concrete, such as the effect of microcracking on expansion strain and microstructure damage on stress relaxation. The damage variables in the examples of previous literature can be summarized into three types. The first one is associated with chemical reactions for the filling of sulfate products and the decalcification of cement-hydrated phases, called chemical damage d_c . The second and third one is both for the stress-induced microcracks, while the sources of stress generated in the concrete are different. In this review, the stress-induced damage related to the interaction between the expansion of sulfate products and the constraint of the cement matrix is called mechanical damage d_m . The stress-induced damage caused by the external loading on the concrete surface is called load damage d_l .

In many studies [92,100,101,103,104], the expansion of the total damage coupled with d_c , d_m , and d_l is proposed according to the theory of continuum damage mechanics as:

$$d_{\text{coup}} = 1 - (1 - d_c)(1 - d_m)(1 - d_l) \tag{15}$$

5.4.1. Chemical Damage

For the d_c , Saetta et al. [100,101] earlier carried out research on the mechanical response of concrete structures under coupled load action and environmental corrosion at 1998 and 1999. They assumed that the chemical damage of concrete caused by an environmental attack (not only for sulfate attack, but also for chloride corrosion, calcium dissolution, etc.) mainly depends on the pollutant concentration of the corrosion ion C and the residual strength of degraded concrete f_{dam} , defined as Equation (19). It is an empirical equation, and the $f_{C-\text{Cref}}$ reflects the degree of chemical reaction, calculated by the ratio of ion concentration C to the reference concentration C_{ref} ($f_{C-\text{Cref}} = C/C_{\text{ref}}$). The $\eta_{R-\text{re}}$ reflects the relative residual strength of the concrete caused by chemical reactions, calculated by the ratio of f_{dam} to the initial strength f_{ini} ($\eta_{R-\text{re}} = f_{\text{dam}}/f_{\text{ini}}$).

Cefis and Comi [92] considered that the decalcification of cement hydrated phases caused by sulfate chemical reactions causes the formation of diffuse microcracks, resulting in the degradation of concrete mechanical properties. In the model, an isotropic chemical damage variable d_c is introduced, which is only related to the extent of the chemical reaction ξ , expressed as Equation (20). Other similar expressions of d_c are shown in Table 7.

5.4.2. Mechanical Damage

For the characterization of d_m , the work performed by Tixier and Mobasher [78] is the earliest and most meaningful, and was developed by many later studies, such as Sarkar et al. [88,89], Yu et al. [64,98,105], Qin et al. [106], Wang et al. [107], Yin et al. [59,96] and Li et al. [108] and is expressed as Equation (22). In this work, a simplified uniaxial tensile stress–strain law was adopted to quantitatively describe the evolution of the damage degree in the process of CSA. The d_m is associated with the free expansive strain ε_V in Equation (6) caused by the formation of sulfate products, namely $d_m \sim \varepsilon_V$. The uniaxial tensile stress–strain curve is divided into three stages, including the linear ascending stage

(LAS), pre-peak non-linear ascending stage (PNAS), and post-peak non-linear descending stage (PNDS). In the CSA process, the initial ε_V is in LAS, meaning that the concrete is undamaged, namely $d_m = 0$. When the increasing ε_V is into PNAS, the microcracks begin to form and spread in the concrete, and the d_m increases linearly. Later, the ε_V increases into PNDS, the microcracks converge into macrocracks, and the d_m has a non-linear rapid increase.

On this basis, Sarkar et al. [88,89] took $d_m \leq d_{crit}$ (d_{crit} is a critical value of concrete failure) as the criterion judge of whether the concrete happens to show surface failure or boundary movement. This work is superior to that of Tixier and Mobasher [78], in which the threshold concentration of reacted calcium aluminate CA was selected to differentiate the cracked and uncracked regions in the concrete. Unfortunately, there is no systematic mechanical analysis in the above research to reveal the essence of mechanical damage, that is, the mechanical interaction between the expansion of sulfate products and the constraint of the concrete matrix.

Therefore, the quantitative method of load damage based on the elastoplastic damage mechanics is used to characterize the stress-induced mechanical damage of concrete under CSA, such as Bary et al. [84,87], Yin et al. [96,102], in which the basic expression of damage is similar to that in Mazars' damage model [109]. The specific equations of mechanical damage are also presented in Table 7. As shown in the table, the difference in the calculation method of I type d_m (d_{m-I}) and II type d_m (d_{m-II}) is whether the calculation can be decoupled. d_{m-I} can be directly calculated by the free volume expansion ε_V from the growth of sulfate products, namely $\varepsilon_V(\xi) \rightarrow d_{m-I}$. d_{m-II} needs to be numerically solved by coupling with stress and strain, and they all need to meet the unified equations, including the equilibrium differential equation, constitutive equation, and geometric equation, as shown in Figure 5.

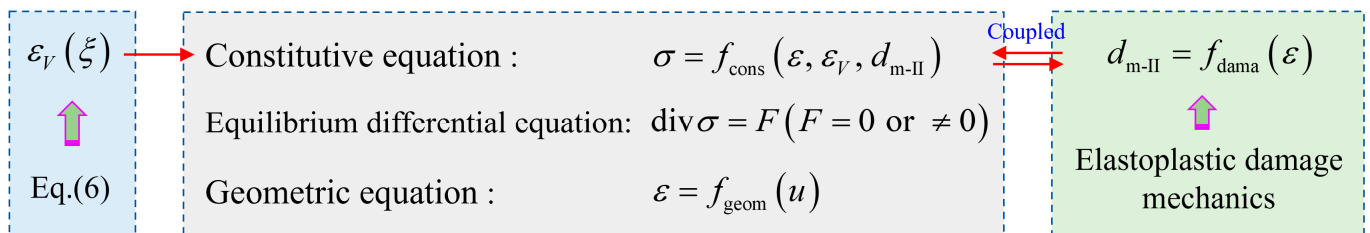


Figure 5. Expressions of damage degree in concrete caused by CSA. Note: f_{cons} , f_{geom} , and f_{dama} are the functions of stress–strain relationship, strain–displacement relationship, and damage degree. F is an external load; u is the displacement.

5.4.3. LOAD DAMAGE

The research on the characterization method of the load-induced damage degree is earlier than the above two, and even part of the research on mechanical damage (namely d_{m-II}) is based on load damage d_l . The achievements of d_l have been quite rich, and they have proposed along with the plasticity or damage constitutive model for the mechanical response in concrete under an external load. The typical constitutive models include Mazars' damage model [109], Lubliner's damage model [110], Faria's rate-independent plasticity damage constitutive model [111], Grassl's damage-plastic model [112,113], and Wu's plastic damage model based on the energy release rate [114]. In these models, the load damage is determined by the damage loading function, the evolution law for the damage variable, and the loading-unloading conditions, as Equations (16)–(18).

$$F_{d-\zeta}(\varepsilon_p, \kappa_{d-\zeta}) = \tilde{\varepsilon}_\zeta(\varepsilon_p) - \kappa_{d-\zeta} \tag{16}$$

$$d_{1-\zeta} = g_d(\kappa_{d-\zeta}) \tag{17}$$

$$F_{d-\zeta} \leq 0, \dot{\kappa}_{d-\zeta} \geq 0, \dot{\kappa}_{d-\zeta} \cdot F_{d-\zeta} = 0 \tag{18}$$

where the subscript $\zeta = (t, c)$ represents the tension and compression condition. $F_{d-\zeta}$ is the damage loading function. $\tilde{\varepsilon}_\zeta$ is the effective stress. $\kappa_{d-\zeta}$ is the damage-driving variable. g_d is the damage function to describe the evolution of the load damage variable.

Generally, two damage parameter variables are adopted to, respectively, describe the damage degree of concrete in two different forms under uniaxial tension and compression. The reason is the different nonlinear (damage) characteristics of concrete under single tension and single compression loads [114]. Therefore, there are two damage driving variables corresponding to the damage variables, namely κ_{d-t} for d_{1-t} and κ_{d-c} for d_{d-c} . The calculation idea of load damage is that the damage-driving variable $\kappa_{d-\zeta}$ is first determined through the damage loading function of Equation (16), in which the plastic strain ε_p can be obtained by the plasticity model. Then, Equation (17) is used to judge the evolution of the damage-driving variable in the whole loading-unloading process. Finally, the load damage degree can be calculated according to the damage function of Equation (17). The expressions of g_d are roughly similar in different constitutive models, as presented in Table 7.

Table 7. Expressions of damage degree in concrete caused by CSA.

| Author | Basic Mechanical Equation | Number |
|---|---|--------|
| Chemical damage d_c | | |
| Saetta et al. [110,111] | $d_c = (1 - \eta_{R-re}) \left[1 - \frac{1}{1 + (2f_{C-Cref})^2} \right]$ <p style="text-align: center;">Related to ion concentration C</p> | (19) |
| Cefis and Comi [92] | $d_c = \frac{1 - \exp(-A_1\tilde{\varepsilon})}{1 + \exp(-A_1\tilde{\varepsilon} + A_2)} A_3$ <p style="text-align: center;">Related to reaction extent</p> | (20) |
| Sun et al. [73] Zhang et al. [115] | $d_c = (1 - \varphi_0) \left[1 - \exp\left(-A_4 \frac{t}{t_0}\right) \right] \left[1 - \frac{1}{1 + A_5 \left(\frac{C}{C_{es0}}\right)^{A_6}} \right]$ <p style="text-align: center;">Related to diffuse time Related to ion concentration C</p> <p>t/t_0 is related to the diffuse time or hydrated time. C/C_0 is the ratio of ion concentration in the concrete to that in the external solution.</p> | (21) |
| Mechanical damage d_m | | |
| Tixier and Mobasher [78] | $d_m = r_7 \cdot \left(1 - \frac{\varepsilon_{th}}{\varepsilon} \right)^{r_8}, \quad \varepsilon = \frac{1}{3}\varepsilon_V$ <p style="text-align: center;">Related to volume expansion</p> <p>ε_{th} is a threshold strain for the initiation of microcracks or damage.</p> | (22) |
| I Wang et al. [116] | $d_m = 1 - \frac{1}{1 + (\zeta - 1) \cdot \left(\frac{\varepsilon}{\varepsilon_m} \right)^{\zeta / (1 - \zeta)}}, \quad \zeta = \frac{E_0}{f_m / \varepsilon_m}$ <p style="text-align: center;">Related to volume expansion</p> <p>E_0 is the initial elastic modulus. ε_m is the ultimate tensile strain corresponding to the ultimate tensile stress f_m at the peak of the stress-strain curve.</p> | (23) |
| Bary et al. [84,87] | $d_m = 1 - \frac{1 - A_9}{\tilde{\varepsilon} / \varepsilon_{th}} - \frac{A_9}{\exp[A_{10}(\tilde{\varepsilon} - \varepsilon_{th})]}$ <p>$\tilde{\varepsilon}$ is the equivalent strain.</p> | (24) |
| II Yin et al. [96,102] | $\begin{cases} d_m = \frac{[\bar{\sigma}^+] d_{m-t} + [\bar{\sigma}^-] d_{m-c}}{ \bar{\sigma} } \\ d_{m-c \text{ or } -t} = 1 - \frac{(1 - A_{11-c \text{ or } -t})}{1 + f(\tilde{\varepsilon}) / \varepsilon_{0-c \text{ or } -t}} - \frac{A_{11-c \text{ or } -t}}{\exp[A_{12-c \text{ or } -t} f(\tilde{\varepsilon}) / \varepsilon_{0-c \text{ or } -t}]} \end{cases}$ <p>$\bar{\sigma}^+$ and $\bar{\sigma}^-$ are the positive and negative spectral decomposition parts of the effective stress tensors $\bar{\sigma}$. $d_{m-c \text{ or } -t}$ is the compressive or tensile stress-induced mechanical damage.</p> | (25) |

Table 7. Cont.

| Author | Basic Mechanical Equation | Number |
|---|--|--------|
| | Load damage d_1 | |
| Grassl et al. [112] | $d_1 = 1 - \exp\left(-\frac{\kappa_d}{\varepsilon_f}\right)$ ε_f is the parameter that controls the slope of the softening curve. | (26) |
| Wu et al. [114] | $d_1^+ = 1 - \frac{r_0^+}{r^+} \exp\left[A_{13}\left(1 - \frac{r^+}{r_0^+}\right)\right]$, $d_1^- = 1 - \frac{r_0^-}{r^-} (1 - A_{14}) - A_{14} \exp\left[A_{15}\left(1 - \frac{r^-}{r_0^-}\right)\right]$ d_1^+ and d_1^- are the tensile damage and shear damage corresponding to positive and negative stress components. | (27) |
| Mazars et al. [109] Zheng et al. [117] | $\begin{cases} d_m = 1 - (1 - s_t d_{1-t})(1 - s_c d_{1-c}) \\ d_{1-c \text{ or } -t} = 1 - \frac{(1 - A_{16-c \text{ or } -t})}{1 + \kappa_{d-c \text{ or } -t} / \varepsilon_{0-c \text{ or } -t}} - \frac{A_{16-c \text{ or } -t}}{\exp(A_{17-c \text{ or } -t} \kappa_{d-c \text{ or } -t} / \varepsilon_{0-c \text{ or } -t})} \end{cases}$ s_t and s_c represent the stiffness recovery effects of tension and compression. | (28) |

$A_{1\sim 16}$ are empirical parameters.

6. Challenges

The above research is aimed at the CSA (transport-chemo-mechanical behavior) on saturated Portland concrete. However, in many service environments, there exists the wetting and drying alternation caused by temperature change, groundwater rising, and falling or tidal fluctuation, resulting in the PSA (transport-physical-mechanical behavior) on unsaturated concrete [118,119]. So, one future challenge is to model the PSA behavior, and it differs from the CSA model in the repeated crystallization-dissolution behavior of sulfate crystal.

The other challenge is to evaluate the CSA-induced durability of cementitious green building materials (CGBMs), such as 3D-printed concrete and recycled aggregate concrete. Due to the printing method, mineral type and content, recycled aggregate quality (loose structure or high sulfate content), 3D-printed concrete [120,121], and recycled aggregate concrete [122,123], low mechanical properties and high porosity may show poor sulfate-resistant properties. At present, relevant research focuses on the effect of these material properties on structural characteristics, while the models to evaluate the durability of CGBMs subjected to CSA are few reported. However, the latter is the key ensuring that the life of CGBMs structures service in sulfate environments.

7. Conclusions

By consulting a lot of research in the literature about chemical sulfate attacks (CSA) on concrete, this review introduces the chemical reaction products of sulfate attack, the formation mechanism of reaction products, them-induced failure forms of concrete, and the model for the whole process of CSA on concrete, step by step. In part of the model, the diffusion-reaction model, chemo-mechanical model, and CSA-induced damage characterization are elaborately detailed. The main conclusions derived from the review are presented as follows:

For the Na^+/K^+ basic ions type CSA, ettringite, gypsum, and thaumasite are the major reaction products. Additionally, the formation mechanism of ettringite and thaumasite is controversial, namely the dispute between the ion-ion reaction and solid-solid reaction.

According to the kind of reaction products, CSA can be classified as gypsum type, ettringite type, and thaumasite type in the case of Na^+/K^+ basic ions and brucite type in the case of Mg^{2+} basic ions. The different types of CSA present different failure forms of the concrete, including softening, cohesiveness, volume expansion, and its-induced cracking/spalling.

For the ettringite type CSA, the theories of volume increase and crystallization pressure are proposed to reveal the degradation mechanism of the concrete. Although the latter, based on thermodynamics, is more scientific, the former, despite lacking a scientific basis, is more widely used in the CSA model because it builds the relationship between the volume expansion of concrete and the content of reaction products.

In order to model the behavior of CSA, the diffusion-reaction models of sulfate are first established to simulate the sulfate transport in the concrete, in which the transport mechanisms, including the ion diffusion, liquid advection, ion–ion interaction, electrical field, and temperature, etc., are considered. However, the diffusion-reaction models cannot analyze the mechanical response in concrete caused by CSA.

On the basis of the diffusion-reaction model and CSA-induced degradation mechanism, the chemo-mechanical models, in which the variables of chemical damage and mechanical damage are introduced, are developed to describe the whole damage process of concrete under CSA. These models can provide a basis for the service life prediction of concrete structures in a sulfate environment. However, the limitation of chemo-mechanical models reported in this review is that these models only apply to the ettringite type CSA on saturated concrete. The model for other types of CSA on unsaturated concrete needs more scholars to invest in this research.

Author Contributions: Writing—Original draft, G.-J.Y. and Y.-J.T.; Foundation support, G.-J.Y., X.-D.W. and Y.-J.T.; Theme determination, X.-D.W.; Investigation, L.M.; Table and Figure Editing, D.C.; Original manuscript modification, X.-B.Z. All authors have read and agreed to the published version of the manuscript.

Funding: This research was funded by the Zhejiang Provincial Natural Science Foundation of China (LQ21E080008), National Natural Science Foundation of China (51569035), Natural Science Foundation of the Jiangsu Higher Education Institutions of China (20KJB430030), Ningbo Scientific and Technological Innovation Major Project in 2025 (2020Z056) and Scientific Research Start-up Foundation of Ningbo University of Technology in 2020.

Institutional Review Board Statement: Not applicable.

Informed Consent Statement: Not applicable.

Data Availability Statement: Not applicable.

Conflicts of Interest: The authors declare no conflict of interest.

References

1. Chen, Z.; Wu, L.; Bindiganavile, V.; Yi, C.F. Coupled models to describe the combined diffusion-reaction behaviour of chloride and sulphate ions in cement-based systems. *Constr. Build. Mater.* **2020**, *243*, 118232. [[CrossRef](#)]
2. Martins, M.C.; Langaro, E.A.; Macioski, G.; Medeiros, M.H.F. External ammonium sulfate attack in concrete: Analysis of the current methodology. *Constr. Build. Mater.* **2021**, *277*, 122252. [[CrossRef](#)]
3. Salt Lake: Accelerating Chinese civilization and creating magnificent scenery. *Chin. Natl. Geogr.* **2011**, *605*, 13.
4. Sun, W. Durability and service life of structure concrete under load and environment coupling effects. *J. Southeast Univ. (Nat. Sci. Ed.)* **2006**, *36* (Suppl. SII), 7–14.
5. Liu, Z.Y. *Study on Methods of Accelerated Testing of Marine Concrete Durability Based on Simulating Environment and Service Life Prediction*; Southeast University: Nanjing, China, 2006.
6. Zhou, G.; Li, S.R.; Wang, Z.J.; Wang, C.F. Investigation and analysis on corrosion situation of concrete in saline soil region. *J. Archit. Civ. Eng.* **2011**, *4*, 121–126.
7. Mehta, P.K. Sulfate attack on concrete: Separating myths from reality. *Concr. Int.* **2000**, *22*, 57–61.
8. Hime, W.G.; Mather, B. "Sulfate attack," or is it. *Cem. Concr. Res.* **1999**, *29*, 789–791. [[CrossRef](#)]
9. Neville, A. The confused world of sulfate attack on concrete. *Cem. Concr. Res.* **2004**, *34*, 1275–1296. [[CrossRef](#)]
10. Neville, A. Consideration of durability of concrete structure: Past, present, and future. *Mater. Struct.* **2001**, *34*, 114–118. [[CrossRef](#)]
11. Bensted, J. Thaumasite-direct, woodfordite and other possible formation routes. *Cem. Concr. Compos.* **2003**, *25*, 873–877. [[CrossRef](#)]
12. Harrison, W.H.; Cooke, R.W. Sulfate resistance of buried concrete. *Proc. Inst. Civ. Eng.* **1981**, *70*, 871–874.
13. Santhanam, M.; Cohen, M.D.; Olek, J. Effects of gypsum formation on the performance of cement mortars during external sulfate attack. *Cem. Concr. Res.* **2003**, *33*, 325–332. [[CrossRef](#)]
14. Tian, B.; Cohen, M.D. Does gypsum formation during sulfate attack on concrete lead to expansion? *Cem. Concr. Res.* **2000**, *30*, 117–123. [[CrossRef](#)]
15. Lee, H.; Cody, R.D.; Cody, A.M.; Spry, P.G. The formation and role of ettringite in Iowa highway concrete deterioration. *Cem. Concr. Res.* **2005**, *35*, 332–343. [[CrossRef](#)]
16. Wang, X.; Pan, Z.; Shen, X.; Liu, W.Q. Stability and decomposition mechanism of ettringite in presence of ammonium sulfate solution. *Constr. Build. Mater.* **2016**, *124*, 786–793. [[CrossRef](#)]

17. Pavoine, A.; Brunetaud, X.; Divet, L. The impact of cement parameters on delayed ettringite formation. *Cem. Concr. Compos.* **2012**, *34*, 521–528. [[CrossRef](#)]
18. Abualgasem, J.M.; Cripps, J.C.; Lynsdale, C.J. Effects of wetting and drying cycles on thaumasite formation in cement mortars. *J. Mater. Civ. Eng.* **2015**, *27*, 1–6. [[CrossRef](#)]
19. Rahman, M.M.; Bassuoni, M.T. Thaumasite sulfate attack on concrete: Mechanisms, influential factors and mitigation. *Constr. Build. Mater.* **2014**, *73*, 652–662. [[CrossRef](#)]
20. Bellmann, F.; Stark, J. Prevention of thaumasite formation in concrete exposed to sulphate attack. *Cem. Concr. Res.* **2007**, *37*, 1215–1222. [[CrossRef](#)]
21. Biczok, I. *Concrete Corrosion Concrete Protection*; Chemical Publishing Company: New York, NY, USA, 1967.
22. Bellmann, F.; Möser, B.; Stark, J. Influence of sulfate solution concentration on the formation of gypsum in sulfate resistance test specimen. *Cem. Concr. Res.* **2006**, *36*, 358–363. [[CrossRef](#)]
23. Ma, B.G.; Luo, Z.T.; Li, X.G.; Gao, X.J.; Zhang, M.X. Microscopic structure and growth mechanism of the corrosion products including thaumasite. *J. Chin. Ceram. Soc.* **2006**, *34*, 1503–1507.
24. Santhanam, M.; Cohen, M.D.; Olek, J. Sulfate attack research—Whither now? *Cem. Concr. Res.* **2001**, *31*, 845–851. [[CrossRef](#)]
25. Bassuoni, M.T.; Nehdi, M.L. Durability of self-consolidating concrete to different exposure regimes of sodium sulfate attack. *Mater. Struct.* **2009**, *42*, 1039–1057. [[CrossRef](#)]
26. Collepardi, M. Thaumasite formation and deterioration in historic buildings. *Cem. Concr. Compos.* **1999**, *21*, 147–154. [[CrossRef](#)]
27. Bonen, D.; Cohen, M.D. Magnesium sulfate attack on Portland cement paste—II. Chemical and mineralogical analyses. *Cem. Concr. Res.* **1992**, *22*, 707–718. [[CrossRef](#)]
28. Durgun, M.Y.; Sevinc, A.H. Determination of the effectiveness of various mineral additives against sodium and magnesium sulfate attack in concrete by Taguchi method. *J. Build. Eng.* **2022**, *57*, 104849. [[CrossRef](#)]
29. Huang, Q.; Zhu, X.H.; Xiong, G.Q.; Zhang, M.T.; Deng, J.X.; Zhao, M.; Zhao, L. Will the magnesium sulfate attack of cement mortars always be inhibited by incorporating nanosilica. *Constr. Build. Mater.* **2021**, *305*, 124695. [[CrossRef](#)]
30. Marchand, J.; Ivan Older Skalny, J.P. *Sulfate Attack on Concrete (Morden Concrete Technology)*; Spon Press: London, UK; New York, NY, USA, 2002.
31. Brown, P.W.; Taylor, H.F.W. *The Role of Ettringite in External Sulfate Attack: Material Science of Concrete—Sulfate Attack Mechanism*; American Ceramic Society: Westerville, OH, USA, 1999.
32. Peng, J.H.; Lou, Z.H. Study Mech. Ettringite Formation. *J. Chin. Ceram. Soc.* **2000**, *28*, 511–515.
33. Evju, C.; Hansen, S. The kinetics of ettringite formation and dilatation in a blended cement with β -hemihydrate and anhydrite as calcium sulfate. *Cem. Concr. Res.* **2005**, *35*, 2310–2321. [[CrossRef](#)]
34. Silva, D.A.; Monteiro, P.J.M. Early Formation of Ettringite in Tricalcium Aluminate-Calcium Hydroxide-Gypsum Dispersions. *J. Am. Ceram. Soc.* **2007**, *90*, 614–617. [[CrossRef](#)]
35. Skalny, J.; Marchand, J.; Odler, I. *Sulfate Attack on Concrete*; Spon Press: London, UK, 2002.
36. Schmidt, T. *Sulfate Attack and the Role of Internal Carbonate on the Formation of Thaumasite*; EPFL: Lausanne, Switzerland, 2007.
37. Yu, C.; Sun, W.; Scrivener, K. Mechanism of expansion of mortars immersed in sodium sulfate solutions. *Cem. Concr. Res.* **2013**, *43*, 105–111. [[CrossRef](#)]
38. Souza, D.J.D.; Medeiros, M.H.F.D.; Filho, J.H. Evaluation of external sulfate attack (Na_2SO_4 and MgSO_4): Portland cement mortars containing fillers. *Rev. IBRACON Estrut. E Mater.* **2020**, *13*, 644–655. [[CrossRef](#)]
39. Collepardi, M. A state-of-the-art review on delayed ettringite attack on concrete. *Cem. Concr. Compos.* **2003**, *25*, 401–407. [[CrossRef](#)]
40. Polivka, M. Factors influencing expansion of expansive cement concretes. *Int. Concr. Abstr. Portal* **1973**, *38*, 239–250.
41. Cohen, M.D. Modeling of expansive cements. *Cem. Concr. Res.* **1983**, *13*, 519–528. [[CrossRef](#)]
42. Cohen, M.D. Theories of expansion in sulfoaluminate—Type expansive cements: Schools of thought. *Cem. Concr. Res.* **1983**, *13*, 809–818. [[CrossRef](#)]
43. Mehta, P.K. Mechanism of expansion associated with ettringite formation. *Cem. Concr. Res.* **1973**, *3*, 1–6. [[CrossRef](#)]
44. Scherer, G.W. Crystallization in pores. *Cem. Concr. Res.* **1999**, *29*, 1347–1358. [[CrossRef](#)]
45. Scherer, G.W. Stress from crystallization of salt. *Cem. Concr. Res.* **2004**, *34*, 1613–1624. [[CrossRef](#)]
46. Clifton, J.R.; Ponnensheim, J.M. *Sulfate Attack of Cementitious Materials: Volumetric Relations and Expansions*; Building and Fire Research, National Institute of Standards and Technology: Gaithersburg, MD, USA, 1994.
47. Lothenbach, B.; Bary, B.; Bescop, P.L.; Schmidt, T.; Letierrier, N. Sulfate Ingress in Portland Cement. *Cem. Concr. Res.* **2010**, *40*, 1211–1225. [[CrossRef](#)]
48. Kunther, W.; Lothenbach, B.; Scrivener, K.L. On the relevance of volume increase for the length changes of mortar bars in sulfate solution s. *Cem. Concr. Res.* **2013**, *46*, 23–29. [[CrossRef](#)]
49. Taylor, H.F.W.; Famy, C.; Scrivener, K.L. Delayed ettringite formation. *Cem. Concr. Res.* **2001**, *31*, 683–693. [[CrossRef](#)]
50. Bizzpzero, J.; Gpsselin, C.; Scrivener, K.L. Expansion mechanisms in calcium aluminate and sulfoaluminate systems with calcium sulfate. *Cem. Concr. Res.* **2014**, *56*, 190–202. [[CrossRef](#)]
51. Metha, P.K. Evaluation of sulfate-resisting cements by a new test method. *J. ACI* **1975**, *72*, 573–575.
52. Steiger, M. Crystal growth in porous materials—II: Influence of crystal size on the crystallization pressure. *J. Cryst. Growth* **2005**, *282*, 470–481. [[CrossRef](#)]

53. Steiger, M. Crystal growth in porous materials—I: The crystallization pressure of large crystals. *J. Cryst. Growth* **2005**, *282*, 455–469. [[CrossRef](#)]
54. Espinosa, R.M.; Franke, L.; Deckelmann, G. Model for the mechanical stress due to the salt crystallization in porous materials. *Constr. Build. Mater.* **2008**, *22*, 1350–1367. [[CrossRef](#)]
55. Koniorczyk, M.; Gawin, D. Modelling of salt crystallization in building materials with microstructure—Poromechanical approach. *Constr. Build. Mater.* **2012**, *36*, 860–873. [[CrossRef](#)]
56. Flatt, R.J. Salt damage in porous materials: How high supersaturations are generated. *J. Cryst. Growth* **2002**, *242*, 435–454. [[CrossRef](#)]
57. Müllauer, W.; Beddoe, R.E.; Heinz, D. Sulfate attack expansion mechanisms. *Cem. Concr. Res.* **2013**, *52*, 208–215. [[CrossRef](#)]
58. Ju, X.D.; Feng, W.J.; Zhang, Y.J. Crystallization stress in brittle porous media. *Chin. J. Geotech. Eng.* **2016**, *38*, 1253–1264.
59. Yin, G.J.; Shan, Z.Q.; Miao, L.; Tang, Y.J.; Zuo, X.B.; Wen, X.D. Finite element analysis on the diffusion-reaction-damage behavior in concrete subjected to sodium sulfate attack. *Eng. Fail. Anal.* **2022**, *137*, 106278. [[CrossRef](#)]
60. Guan, B.W.; Liu, J.N.; Wu, J.W.; Chen, X.H.; Hu, Y.; Zhang, L.Q. Transport behavior of sulfate ions in concrete with attack damage. *Bull. Chin. Ceram. Soc.* **2020**, *39*, 3169–3174.
61. Zhao, S.B.; Yang, X.M. Experimental study on regularity of sulfate-ion diffusion and distribution in concrete attacked by sulfate. *China Harb. Eng.* **2009**, *161*, 26–29.
62. Ran, B.; Li, K.F.; Teddy, F.C.; Omikrine-Metalssi, O.; Dangka, P. Spalling rate of concretes subject to combined leaching and external sulfate attack. *Cem. Concr. Res.* **2022**, *162*, 106951. [[CrossRef](#)]
63. Zou, D.J.; Qin, S.S.; Liu, T.J.; Jivkov, A. Experimental and numerical study of the effect of solution concentration and temperature on concrete under external sulfate attack. *Cem. Concr. Res.* **2021**, *139*, 106284. [[CrossRef](#)]
64. Yu, Y.; Zhang, Y.X. Numerical modelling of mechanical deterioration of cement mortar under sulfate attack. *Constr. Build. Mater.* **2018**, *158*, 490–502. [[CrossRef](#)]
65. Shazail, M.A.; Baluch, M.H.; Al-Gadhib, A.H. Predicting residual strength in unsaturated concrete exposed to sulfate attack. *J. Mater. Civil Eng.* **2006**, *18*, 343–354. [[CrossRef](#)]
66. Gospodinov, P.; Kazandjiev, R.; Mironova, M. The effect of sulfate ion diffusion on the structure of cement stone. *Cem. Concr. Compos.* **1996**, *18*, 401–407. [[CrossRef](#)]
67. Gospodinov, P.N.; Kazandjiev, R.F.; Partalin, T.A.; Mironovac, M.K. Diffusion of sulfate ions into cement stone regarding simultaneous chemical reactions and resulting effects. *Cem. Concr. Res.* **1999**, *29*, 1591–1596. [[CrossRef](#)]
68. Gospodinov, P.N. Numerical simulation of 3D sulfate ion diffusion and liquid push out of the material capillaries in cement composites. *Cem. Concr. Res.* **2005**, *35*, 520–526. [[CrossRef](#)]
69. Marchand, J.; Samson, E.; Maltais, Y.; Beaudoin, J.J. Theoretical analysis of the effect of weak sodium sulfate solutions on the durability of concrete. *Cem. Concr. Compos.* **2002**, *24*, 317–329. [[CrossRef](#)]
70. Liu, X.; Liu, Q.W.; Wang, S.G.; Xu, F.; Han, J.D. Recent development on theoretical models of sulfate attack on concrete. *Mater. Rev.* **2014**, *28*, 89–95.
71. Zuo, X.B.; Sun, W.; Li, H.; Zhao, Y.K. Modeling of diffusion-reaction behavior of sulfate ion in concrete under sulfate environments. *Comput. Concr.* **2012**, *10*, 47–51. [[CrossRef](#)]
72. Sun, W.; Zuo, X.B. Numerical simulation of sulfate diffusivity in concrete under combination of mechanical loading and sulfate environments. *J. Sustain. Cem.-Based Mater.* **2012**, *1*, 46–55. [[CrossRef](#)]
73. Sun, C.; Chen, J.K.; Zhu, J.; Zhang, M.H.; Ye, J. A new diffusion model of sulfate ions in concrete. *Constr. Build. Mater.* **2013**, *39*, 39–45. [[CrossRef](#)]
74. Yang, C.C.; Su, J.K. Approximate migration coefficient of interfacial transition zone and the effect of aggregate content on the migration coefficient of mortar. *Cem. Concr. Res.* **2002**, *32*, 1559–1565. [[CrossRef](#)]
75. Yang, C.C.; Cho, S.W. Approximate migration coefficient of percolated interfacial transition zone by using the accelerated chloride migration test. *Cem. Concr. Res.* **2005**, *35*, 344–350. [[CrossRef](#)]
76. Huang, Q.H.; Zhou, C.Z.; Gu, X.L.; Zhang, W.P. Experimental study on moisture transport property of interfacial transition zone in concrete. *J. Build. Struct.* **2019**, *40*, 174–180.
77. Atkinson, A.; Hearne, J.A. Mechanistic model for the durability of concrete barriers exposed to sulphate-bearing groundwaters. *Mrs. Proc.* **1989**, *176*, 149–156. [[CrossRef](#)]
78. Tixier, R.; Mobasher, B. Modeling of Damage in cement-based materials subjected to external sulfate attack. I: Formulation. *J. Mater. Civ. Eng.* **2003**, *15*, 305–313. [[CrossRef](#)]
79. Basista, M.; Weglewski, W. Chemically Assisted Damage of Concrete: A Model of Expansion Under External Sulfate Attack. *Int. J. Damage Mech.* **2009**, *18*, 155–175. [[CrossRef](#)]
80. Idiart, A.E.; López, C.M.; Carol, I. Chemo-mechanical analysis of concrete cracking and degradation due to external sulfate attack: A meso-scale model. *Cem. Concr. Compos.* **2011**, *33*, 411–423. [[CrossRef](#)]
81. Ikumi, T.; Cavalario, S.H.P.; Segura, I.; Aguado, A. Alternative methodology to consider damage and expansions in external sulfate attack modeling. *Cem. Concr. Res.* **2014**, *63*, 105–116. [[CrossRef](#)]
82. Yu, C.; Sun, W.; Scrivener, K.L. Degradation mechanism of slag blended mortars immersed in sodium sulfate solution. *Cem. Concr. Res.* **2015**, *72*, 37–47. [[CrossRef](#)]

83. Yin, G.J.; Zuo, X.B.; Sun, X.; Tang, Y.J. Macro-microscopically numerical analysis on expansion response of hardened cement paste under external sulfate attack. *Constr. Build. Mater.* **2019**, *207*, 600–615. [[CrossRef](#)]
84. Bary, B. Simplified coupled chemo-mechanical modeling of cement pastes behavior subjected to combined leaching and external sulfate attack. *Int. J. Numer. Anal. Methods Geomech.* **2008**, *32*, 1791–1816. [[CrossRef](#)]
85. Feng, P.; Bullard, J.W.; Garboczi, E.J. A multiscale microstructure model of cement paste sulfate attack by crystallization pressure. *Modelling Simul. Mater. Sci. Eng.* **2017**, *25*, 65013.
86. Tixier, R.; Mobasher, B. Modeling of Damage in Cement-Based Materials Subjected to External Sulfate Attack. II: Comparison with experiments. *J. Mater. Civ. Eng.* **2003**, *15*, 314–322. [[CrossRef](#)]
87. Bary, B.; Leterrier, N.; Deville, E.; Bescop, P. Coupled chemo-transport-mechanical modelling and numerical simulation of external sulfate attack in mortar. *Cem. Concr. Compos.* **2014**, *49*, 70–83. [[CrossRef](#)]
88. Sarkar, S.; Mahadevan, S.; Meeussen, J.C.L.; Sloot, H.V.D.; Kosson, D.S. Numerical simulation of cementitious materials degradation under external sulfate attack. *Cem. Concr. Compos.* **2010**, *32*, 241–252. [[CrossRef](#)]
89. Sarkar, S.; Mahadevan, S.; Meeussen, J.C.L.; Sloot, S.V.D.; Kosson, D.S. Sensitivity Analysis of Damage in Cement Materials under Sulfate Attack and Calcium Leaching. *J. Mater. Civ. Eng.* **2012**, *24*, 430–440. [[CrossRef](#)]
90. Ikumi, T.; Cavalaro, S.H.P.; Segura, I.; Fuente, A.D.L.; Aguado, A. Simplified methodology to evaluate the external sulfate attack in concrete structures. *Mater. Des.* **2016**, *89*, 1147–1160. [[CrossRef](#)]
91. Cefis, N.; Comi, C. Damage modelling in concrete subject to sulfate attack. *Frat. Integrità Strutt.* **2014**, *8*, 222–229. [[CrossRef](#)]
92. Cefis, N.; Comi, C. Chemo-mechanical modelling of the external sulfate attack in concrete. *Cem. Concr. Res.* **2017**, *93*, 57–70. [[CrossRef](#)]
93. Zuo, X.B.; Sun, W. Full process analysis of damage and failure of concrete subjected to external sulfate attack. *J. Chin. Ceram. Soc.* **2009**, *37*, 1063–1067.
94. Zuo, X.B.; Sun, W.; Yu, C. Numerical investigation on expansive volume strain in concrete subjected to sulfate attack. *Constr. Build. Mater.* **2012**, *36*, 404–410. [[CrossRef](#)]
95. Nie, Q.; Zhou, C.; Li, H.; Sun, X.; Gong, H.; Huang, B. Numerical simulation of fly ash concrete under sulfate attack. *Constr. Build. Mater.* **2015**, *84*, 261–268. [[CrossRef](#)]
96. Yin, G.J.; Zuo, X.B.; Tang, Y.; Tang, Y.J. Numerical simulation on time-dependent mechanical behavior of concrete under coupled axial loading and sulfate attack. *Ocean Eng.* **2017**, *142*, 115–124. [[CrossRef](#)]
97. Yin, G.J.; Zuo, X.B.; Sun, X.; Tang, Y.J. Numerical investigation on ESA-induced expansion response of cement paste by using crystallization pressure. *Model. Simul. Mater. Sci. Eng.* **2019**, *27*, 25006. [[CrossRef](#)]
98. Yu, Y.G.; Gao, W.; Feng, Y.; Gastel, A.; Chen, X.J.; Liu, A.R. On the competitive antagonism effect in combined chloride-sulfate attack A numerical exploration. *Cem. Concr. Res.* **2021**, *144*, 106406. [[CrossRef](#)]
99. Yi, C.F.; Zheng, C.; Vivek, B. A non-homogeneous model to predict the service life of concrete subjected to external sulfate attack. *Constr. Build. Mater.* **2019**, *212*, 254–265. [[CrossRef](#)]
100. Saetta, A.; Scotta, R.; Vitaliani, R. Mechanical Behavior of Concrete under Physical-Chemical Attacks. *J. Eng. Mech.* **1998**, *124*, 1100–1109. [[CrossRef](#)]
101. Saetta, A.; Scotta, R.; Vitaliani, R. Coupled Environmental-Mechanical Damage Model of RC Structures. *J. Eng. Mech.* **1999**, *125*, 930–940. [[CrossRef](#)]
102. Yin, G.J.; Zuo, X.B.; Li, X.N.; Zou, Y.X. An integrated macro-microscopic model for concrete deterioration under external sulfate attack. *Eng. Fract. Mech.* **2020**, *240*, 107345. [[CrossRef](#)]
103. Li, R.T.; Li, X.K. A coupled chemo-elastoplastic-damage constitutive model for plain concrete subjected to high temperature. *Int. J. Damage Mech.* **2010**, *19*, 971–1000.
104. Yin, G.J.; Zuo, X.B.; Tang, Y.; Olawale, A.; Ding, D.N. Modeling of time-varying stress in concrete under axial loading and sulfate attack. *Comput. Concr.* **2017**, *19*, 143–152. [[CrossRef](#)]
105. Yu, Y.G.; Gao, W.; Castel, A.; Liu, A.; Chen, X.J.; Liu, M. Assessing external sulfate attack on thin-shell artificial reef structures under uncertainty. *Ocean Eng.* **2020**, *207*, 107397. [[CrossRef](#)]
106. Qin, S.; Zhou, D.; Liu, T.; Jiv, A. A chemo-transport-damage model for concrete under external attack. *Cem. Concr. Res.* **2020**, *132*, 106048. [[CrossRef](#)]
107. Wang, P.; Mo, R.; Li, S.; Xu, J.; Jin, Z.Q.; Zhao, T.J.; Wang, D.Z. A chemo-damage-transport model for chloride ions diffusion in cement-based materials: Combined effects of sulfate attack and temperature. *Constr. Build. Mater.* **2021**, *288*, 123121. [[CrossRef](#)]
108. Li, J.P.; Xie, F.; Zhao, G.W.; Li, L. Experimental and numerical investigation of cast-in-situ concrete under external sulfate attack and drying-wetting cycles. *Constr. Build. Mater.* **2020**, *249*, 118789. [[CrossRef](#)]
109. Mazars, J.; Pyaudier-Cabot, G. Continuum damage theory-application to concrete. *J. Eng. Mech.* **1989**, *115*, 345–365. [[CrossRef](#)]
110. Lubliner, J.; Oliver, J.; Oller, S.; Onate, E. A plastic-damage model for concrete. *Int. J. Solids Struct.* **1989**, *25*, 299–326. [[CrossRef](#)]
111. Faria, R.; Oliver, J.; Cervera, M. A strain-based plastic viscous-damage model for massive concrete structures. *Int. J. Solids Struct.* **1998**, *35*, 1533–1558. [[CrossRef](#)]
112. Grassl, P.; Jirásek, M. Damage-plastic model for concrete failure. *Int. J. Solids Struct.* **2006**, *43*, 7166–7196. [[CrossRef](#)]
113. Grassl, P.; Xenos, D.; Nyström, U.; Rempling, R.; Gylltoft, K. CDPM2, A damage-plasticity approach to modelling the failure of concrete. *Int. J. Solids Struct.* **2013**, *50*, 3805–3816. [[CrossRef](#)]

114. Wu, J.Y.; Li, J.; Faria, R. An energy release rate-based plastic-damage model for concrete. *Int. J. Solids Struct.* **2006**, *43*, 583–612. [[CrossRef](#)]
115. Zhang, C.L.; Chen, W.K.; Mu, S.; Savija, B.; Liu, Q.F. Numerical investigation of external sulfate attack and its effect on chloride binding and diffusion in concrete. *Constr. Build. Mater.* **2021**, *285*, 122806. [[CrossRef](#)]
116. Wang, H.L.; Chen, Z.; Li, H.; Sun, X.Y. Numerical simulation of external sulphate attack in concrete considering coupled chemo-diffusion-mechanical effect. *Constr. Build. Mater.* **2021**, *292*, 123325. [[CrossRef](#)]
117. Zheng, F.; Wu, Z.; Gu, C.; Bao, T.F.; Hu, J. A plastic damage model for concrete structure cracks with two damage variables. *Sci. China Technol. Sci.* **2012**, *55*, 2971–2980. [[CrossRef](#)]
118. Silva, D.; Fajardo-San-Miguel, G.; Escadeillas, G.; Cruz-Moreno, D. Surface treatment with silicon-based nanoparticles in Portland cement specimens subjected to physical sulfate attack. *Case Stud. Constr. Mater.* **2023**, *18*, e01795. [[CrossRef](#)]
119. Esselami, R.; Wilson, W.; Tagni-Hamou, A. An accelerated physical sulfate attack test using an induction period and heat drying: First applications to concrete with different binders including ground glass pozzolan and limestone filler. *Constr. Build. Mater.* **2022**, *345*, 128046. [[CrossRef](#)]
120. Singh, A.; Liu, Q.; Xiao, J.Z.; Lyu, Q.F. Mechanical and macrostructural properties of 3D printed concrete dosed with steel fibers under different loading direction. *Constr. Build. Mater.* **2022**, *323*, 126616. [[CrossRef](#)]
121. Khosravani, M.R.; Haghighi, A. Large-scale automated additive construction: Overview, robotic solutions, sustainability, and future prospect. *Sustainability* **2022**, *14*, 9872. [[CrossRef](#)]
122. Waseem, S.A.; Singh, B. An experimental study on shear capacity of interfaces in recycled aggregate concrete under multiaxial compression. *Struct. Concr.* **2018**, *19*, 230–245. [[CrossRef](#)]
123. Zhou, J.H.; Kang, T.B.; Wang, F.C. Pore structure and strength of waste fiber recycled concrete. *J. Eng. Fibers Fabr.* **2019**, *14*, 1–10. [[CrossRef](#)]

Disclaimer/Publisher's Note: The statements, opinions and data contained in all publications are solely those of the individual author(s) and contributor(s) and not of MDPI and/or the editor(s). MDPI and/or the editor(s) disclaim responsibility for any injury to people or property resulting from any ideas, methods, instructions or products referred to in the content.